Isolated Attosecond Pulse Generation without the Need to Stabilize the Carrier-Envelope Phase of Driving Lasers

Steve Gilbertson,[1] Sabih D. Khan,[1] Yi Wu,[1] Michael Chini,[1] and Zenghu Chang[1,2,*]

[1]*Department of Physics, Kansas State University, Manhattan, Kansas 66506, USA*

[2]*CREOL and Department of Physics, University of Central Florida, Orlando, Florida 32816, USA*

(Received 10 March 2010; published 24 August 2010)

Single isolated attosecond pulses can be extracted from a pulse train with an ultrafast gate in the generation target. By setting the gate width sufficiently narrow with the generalized double optical gating, we demonstrate that single isolated attosecond pulses can be generated with any arbitrary carrier-envelope phase value of the driving laser. The carrier-envelope phase only affects the photon flux, not the pulse duration or contrast. Our results show that isolated attosecond pulses can be generated using carrier-envelope phase unstabilized 23 fs pulses directly from chirped pulse amplifiers.

DOI: 10.1103/PhysRevLett.105.093902 PACS numbers: 42.65.Re, 32.80.Qk, 42.65.Ky

Since single attosecond pulses were first demonstrated, great advances have been made in reducing the pulse duration [1] and applying the pulses to various experiments with atoms, molecules, and solids [2]. It is still a technical challenge to generate such pulses, however, and as a consequence very few labs have been able to probe attosecond dynamics. The main limitations have been the requirements on the input pulse duration and the stability of the carrier-envelope (CE) phase of the generating laser. The attosecond pulse generation methods of amplitude gating [3] and polarization gating [4] both require few cycle laser pulses ideally <5 fs in duration. Additionally, locking the CE phase of a few mJ laser system is nontrivial. These two requirements are beyond the capabilities of many labs. Furthermore, to scale up the photon flux, one wishes to use pettawatt (PW) class lasers. However, due to large power fluctuations and low repetition rate, locking the CE phase of such ultrahigh power lasers has not been demonstrated.

Recently, the method of double optical gating (DOG) was demonstrated to be capable of generating attosecond pulses from multicycle lasers [5]. Consequently, the possibility for generating attosecond pulses became more feasible. Later, the generalized version of DOG (GDOG) was demonstrated for generating attosecond pulses directly from chirped pulse amplifiers [6]. This allows any laser system capable of 28 fs pulse duration or less the opportunity to generate isolated attosecond pulses.

The other requirement, which is CE phase stability, has still remained a problem, however. All of the current attosecond pulse generation schemes rely on gating a single attosecond pulse from a pulse train by effectively reducing the generation laser to pulse durations on the order of the attosecond pulse train period. Since CE phase fluctuations play a large role in the attosecond pulse number per shot [5], locking the CE phase to a known offset value is critical to the quality of pulses produced. In previous experiments, the ''gate width.'' or region of the generating laser that produces the attosecond burst of photons, was set to be equal to the attosecond pulse train period. For amplitude gating and polarization gating, this is half of an optical cycle of the fundamental laser period, and for DOG and GDOG this is one optical cycle. Once the gate width is set, the CE phase is locked so that the most efficient pulse with the smoothest spectrum is generated. For other phase values, two attosecond pulses per shot can be generated. In this work, we demonstrate that only one isolated attosecond pulse can be produced if the gate width is sufficiently narrow, no matter what the CE phase values are.

Experimentally the GDOG field, produced with birefringent optics [6], consists of two counterrotating laser pulses with some amount of delay T_d between them. This generates a pulse with a time varying ellipticity with a short linearly polarized portion in the center known as the polarization gate width [7]. The attosecond pulse generation process [8] can only efficiently occur inside the gate. To the ellipticity varying pulse, a weak second harmonic field is superimposed to break the symmetry of the linear gate width, thereby increasing the separation of the attosecond pulse train from half of a laser optical cycle to one cycle. The gate width is expressed by the following equation [6]:

$$\delta t_G \approx 0.3 \frac{\varepsilon \tau_p^2}{T_d}. \quad (1)$$

Here, τ_p is the pulse duration of the generating laser, T_d is the delay between the two initial counterrotating pulses, and ε is the ellipticity of the counterrotating pulses. For GDOG, ε is typically 0.5.

In our previous GDOG work, the gate width was set equal to one optical cycle, or $\sim$2.5 fs. This is the upper limit for generating isolated attosecond pulses with a proper CE phase. The gate width can be further reduced by tuning any of the parameters in the equation so that it is much less than one optical cycle. Figures 1(a) and 1(b) show the electric field of the driving laser with two values of the CE phase within the gate. The color gradient indicates the ellipticity of the generating laser pulse with white being the most linear. Here, the gate width was

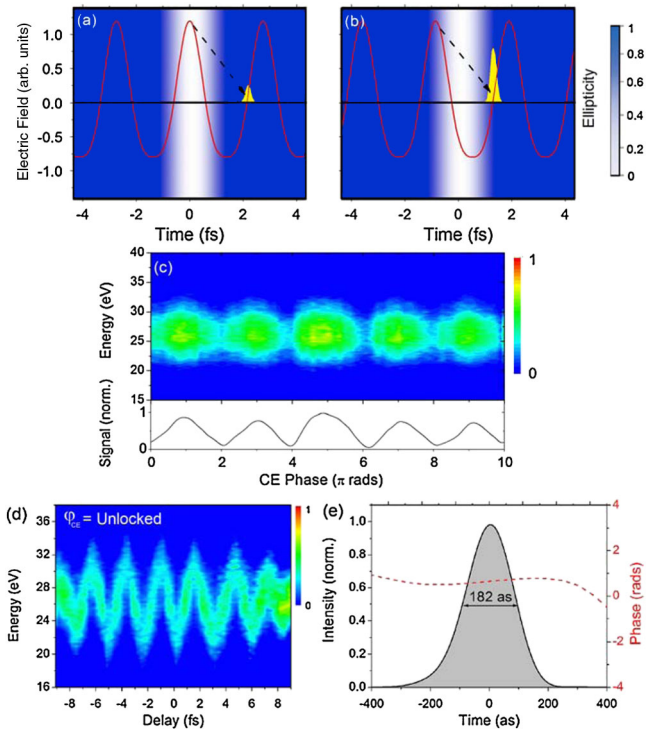

FIG. 1 (color online). The effect of a narrow gate width (~1 fs) on the generated attosecond pulse. In (a), the CE phase of the NIR laser means the freed electron recombines in a field of high ellipticity, severely limiting its recombination probability. In (b), the CE phase is more favorable for high attosecond pulse emission since the electron experiences a linear field for its full lifetime. The color gradient represents the ellipticity of the field with the darker being the most elliptical and white the most linear. The experimental evidence for this effect is shown in (c). The upper figure shows the energy spectrum as a function of the CE phase of the NIR laser while the lower plot shows the total signal integrated along the energy axis. The 2π periodic structure is the effects of the two-color gating in GDOG. (d) A streaked spectrogram when the CE phase is unlocked. (e) The temporal profile (solid line) and phase (dashed line) for the pulse shown in (d).

chosen to be ~1 fs (about half of a laser cycle) and is where the attosecond pulse is produced via the three-step model [9]. In 1(a), the electron is born during a strongly linearly polarized field but recombines in a field that is increasingly elliptical. This reduces the recombination probability. In 1(b), the electron spends all of its excursion time away from the nuclear core in a mainly linearly polarized field meaning the attosecond photon flux should be maximized. In both cases, since the gate width is much smaller than the spacing between two possible adjacent attosecond pulses, it is not possible to generate two attosecond pulses per laser shot.

Figure 1(c) shows the experimental evidence for this effect. For this portion of the experiment, a 9 fs laser pulse was produced by 2 mJ, 25 fs pulses from the Kansas Light Source passing through a Ne filled hollow-core fiber and chirped mirrors compressor. The laser power fluctuation was recorded as being less than 1%. This beam then passed through the GDOG optics [6] consisting of a 530 μm quartz plate (5 cycle delay T_d), a 0.5 mm Brewster window, and a 440 μm quartz plate and 141 μm barium borate crystal (BBO), and was focused by an $f = 375$ mm focal length spherical mirror into a 1.4 mm long Ar gas filled target. The gate width for these parameters was calculated to be ~1.4 fs.

The attosecond extreme ultraviolet (XUV) beam then propagated to the central mirror of a two component mirror, which is a Mo/Si spherical mirror with focal length $f = 250$ mm. The beam was then focused to a second 50 μm diameter gas jet filled with Kr gas. This converted the photon burst into a replica photoelectron burst which was then detected by a position-sensitive time of flight (TOF) detector. The energy resolution of the TOF was ~400 meV in this energy range [10], which is much smaller than the photon energy of the driving laser (1.5 eV). Details of the setup are given in Ref. [8].

The intensity plot in Fig. 1(c) shows the energy spectrum of the burst of photoelectrons liberated by an attosecond burst of XUV photons as a function of the CE phase of the input generating laser. The CE phase was continuously shifted from 0 to 2π by shifting the gratings in our stretcher [11] through feedback control of a fringe pattern generated in an f-to-$2f$ interferometer while the relative CE phase values were monitored and recorded. Typically, the CE phase stability is better than 250 mrad after the hollow-core fiber [12]. Two features of the spectrogram are obvious. First, the spectrum is a continuum for all CE phase values, which satisfies the necessary condition for generating isolated attosecond pulses. Second, the intensity of the spectrum strongly depends on the CE phase, which is expected for such a narrow gate width.

The plot in Fig. 1(c) shows the signal of the CE phase integrated along the energy spectrum. The modulation depth is an indication of the width of the linear polarization. For narrower gate widths, the modulation depth would become even stronger, while for wider gate widths the modulation would become shallower, and eventually the energy spectrum would exhibit modulations indicative of multiple pulses within the gate width [6].

Spectral measurements alone, of course, cannot fully characterize the attosecond pulse temporal profile. In order to accomplish this, we used the attosecond streaking technique [1,13]. In fact, Fig. 1(c) was obtained with the generation arm of an interferometric streak camera. A linearly polarized near-infrared (NIR) laser was sent to the streaking arm for the temporal measurement of the XUV pulse. After the interferometer, the two beams propagated collinearly to the two components mirror. The NIR photons reflected from the outer spherical silver mirror. The two beams were overlapped at the second gas jet so that the attosecond XUV burst generated photoelectrons and the NIR pulse gave a momentum shift to the freed electrons. The inner mirror of the two component mirror system was mounted on a piezoelectric transducer stage so

that temporal delay could be introduced between the NIR and XUV pulses. The spectrum of emitted photoelectrons was then recorded as a function of the delay between the two beams with the position-sensitive TOF.

The photoelectron detector of the streak camera is oriented horizontally and is parallel to the input laser polarization. To ensure the polarization of the linearly polarized portion of the ellipticity varying pulse is also parallel to the TOF detector axis, the plates of GDOG must be chosen correctly. The first plate is a full-wave plate which ensures that the portion of the field that generates the attosecond flux later is parallel to the detector axis. The second quartz plate and BBO crystal have their optical axes in the plane containing the TOF axis. This ensures the linear part of the GDOG pulse is aligned along the TOF axis as well. Also, due to the large acceptance angle of the detector ($\pm 14°$ at 45 eV), even photoelectrons that could be generated from the edges of the polarization gate where the field ellipticity is 0.2 are still collected since the angle between the laser field and TOF axis is $\pm 11.3°$.

Figure 1(d) shows a streaked spectrogram for a pulse when the CE phase is unlocked. This image exhibits an extra NIR laser cycle as would be expected when the CE phase is locked since the envelope can shift over one full optical cycle. The carrier of the laser field is not smeared out since the attosecond pulse is temporally locked to the driving laser oscillation. The temporal profile as reconstructed from the frequency resolved optical gating for the complete reconstruction of attosecond bursts (FROGCRAB) method [14] is shown as the solid line in Fig. 1(e) while the temporal phase is shown as the dashed line. The pulse duration was found to be ~ 182 as.

The reconstruction of the attosecond pulse using CE phase unlocked lasers assumed that the temporal profile and phase of the attosecond pulse does not change CE phase. To make sure this is true, streaked spectrograms for four different values of the CE phase on the input laser were taken, as Fig. 2 shows. The CE phase was locked to ~ 200 mrad through feedback control of the grating separation in the stretcher of the amplifier for 15 min intervals (~ 20 s per delay slice) while the streaked spectrogram was generated. All the figures are normalized to the counts of Fig. 2(c). The differences in count rates are attributed to the different values of the CE phase and hence the different fluxes of the attosecond pulse emission. This is the same as locking the CE phase at various slices from Fig. 1(c) and then taking a full streaked spectrogram at each. Figure 3(a) shows the spectrum for each value of the CE phase. Figures 3(b) and 3(c) show the temporal profiles (solid lines) and phases (dashed lines) for the spectrograms in Fig. 2 as reconstructed with FROGCRAB method. The profiles were separated into two figures for clarity. Finally, each streaked spectrogram was Fourier filtered to extract the oscillating NIR field. Figure 3(d) shows the results. In this case the CE phase of the 9 fs laser pulse can be easily seen with (for example) Figs. 2(a) and 2(c) showing a π shift. One should keep in mind that the CE phase of the generating pulse is locked to the streaking pulse as the CE phase was stabilized and varied upstream. Their absolute values are different, though, because the dispersion is not the same in the two paths.

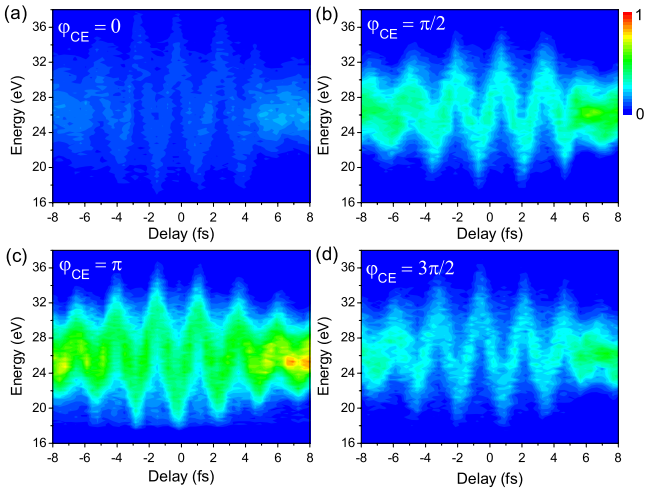

FIG. 2 (color online). Streaked photoelectron spectrograms for four different values of the CE phase. (a) ~ 0 rad, (b) $\sim \pi/2$ rad, (c) $\sim \pi$ rad, and (d) $\sim 3\pi/2$ rad. The images are normalized to the peak counts of (c).

The peak number of counts of each spectrogram was sufficient for reconstruction [15]. This allowed the accurate reconstruction for each with the pulse durations being

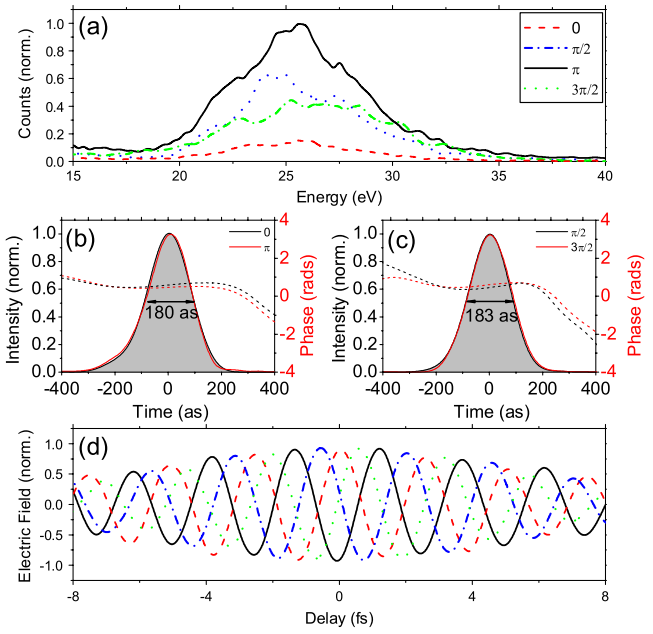

FIG. 3 (color online). (a) The photoelectron energy spectrum for each of the streaked spectrograms of Fig. 2. (b) The temporal profiles (solid lines) and phases (dashed lines) for the spectrograms with phase 0 (black line) and π [gray (red) line]. (c) The temporal profiles and phases for the spectrograms with phase $\pi/2$ (black line) and $3\pi/2$ [gray (red) line]. Each line corresponds to the spectra from (a). Panel (d) shows the extracted electric fields of each of the spectrograms from Fig. 2.

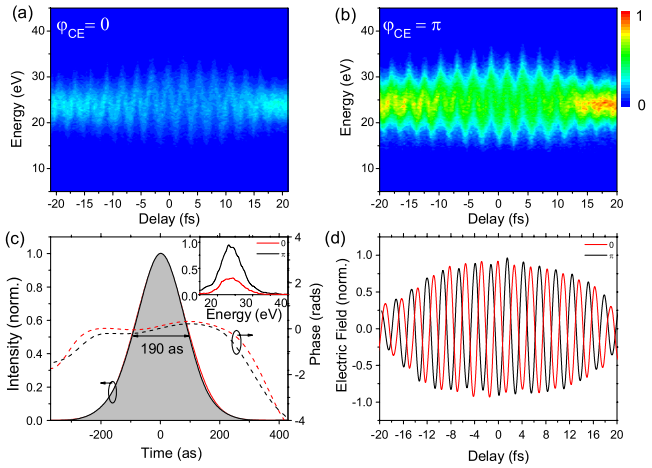

FIG. 4 (color online). (a),(b) Streaked spectrograms of attosecond pulses produced directly from an amplifier with an approximately π shift between them. Panel (c) shows the temporal profiles of (a) and (b) while the inset shows the energy spectrum of (a) [gray (red) line] and (b) (black line). The electric fields extracted from (a) and (b) through Fourier filtering is shown in (d) for the phase of 0 gray (red) line] and π (black line).

$\sim$180 as for each. The results have less than 5% error between each case, implying that the CE phase does not need to be stabilized to generate the same attosecond pulse provided the gate width is narrow enough. The ratio between the main pulse and the pre- or postpulses is $\sim 10^{-5}$ for the four cases.

Next, attosecond pulses were produced from 23 fs laser pulses directly from the amplifier [6]. The GDOG optics were identical to the short pulse case with the exception that the first quartz plate was 1950 μm thick corresponding to 22 cycles of delay and yielding a $\sim$2 fs gate width. Figures 4(a) and 4(b) show streaked spectrograms for two different values of the CE phase. Again, the count rate is reduced between the two cases. Figure 4(c) shows the temporal profiles (solid lines) and phases (dashed lines) for the two cases. Both have near identical durations of $\sim$190 as and phase shapes. The inset in Fig. 4(c) shows the energy spectrum for the two phases. The signal ratio between the two cases is not as extreme as the short pulse case. This can be explained by the gate width being slightly wider than the short pulse case. The NIR laser pulse from the Fourier filtering of the streaked spectrograms is indicated in Fig. 4(d). This is in excellent agreement with the CE phase unlocked reconstruction of 190 as.

In conclusion, we have demonstrated that isolated attosecond pulses can be generated from lasers with unstabilized CE phase using the GDOG method. If the gate width is sufficiently narrow, the attosecond pulses produced at different CE phase values are always identical to each other except for the photon flux. This is true for both 9 and 23 fs lasers. The 23 fs NIR pulses were produced directly from a chirped pulse amplifier. Interestingly, applying the same idea to gating schemes that use the fundamental laser field only will not work well. In that case, the attosecond pulse spacing is half of a laser cycle. One may think of reducing the gate width to a quarter of the laser cycle to accomplish the same as what the GDOG does; however, that is too short because it takes one half laser cycle for the electron to return to the parent ion.

The ability to generate isolated attosecond pulses without the need to lock the CE phase opens the door for the generation of high flux attosecond pulses with PW class lasers that do not have the ability to stabilize the CE phase [16], which is crucial for investigating attosecond nonlinear processes. Because of the energy, beam size, and repetition rate differences between PW and mJ lasers, implementing the GDOG technique using such large scale lasers may not be straightforward, with many details yet to be worked out. To achieve the same NIR intensity on the target as in the current work so that the same ionization probability and coherence length are maintained, the laser spot size must be much larger when PW lasers are used. The up-scaling of the attosecond pulse energy comes from the scaling of the transverse spot size with the laser energy. Since the PW laser pulse duration is longer than 20 fs, the ionization probability is high even with GDOG. Quasi-phase matching techniques have been demonstrated to improve the conversion efficiency of high harmonic generation in highly ionized gases [17,18]. Some of these schemes, such as modulating the gas density, can be combined with GDOG for further enhancements of the photon flux. It could be easier to configure the gas modulation density distribution in the propagation direction in the PW case because of the long Rayleigh range.

This material is supported by the ARO MURI of the U.S. Department of Defense and by the U.S. Department of Energy.

*zechang@mail.ucf.edu

[1] E. Gouliemakis *et al.*, Science **320**, 1614 (2008).
[2] A. Scrinzi *et al.*, J. Phys. B **39**, R1 (2006).
[3] A. Baltuska *et al.*, Nature (London) **421**, 611 (2003).
[4] G. Sansone *et al.*, Science **314**, 443 (2006).
[5] H. Mashiko *et al.*, Phys. Rev. Lett. **100**, 103906 (2008).
[6] X. Feng *et al.*, Phys. Rev. Lett. **103**, 183901 (2009).
[7] P. B. Corkum, N. H. Burnett, and M. Y. Ivanov, Opt. Lett. **19**, 1870 (1994).
[8] B. Shan, S. Ghimire, and Zenghu Chang, Phys. Rev. A **69**, 021404 (2004).
[9] P. B. Corkum, Phys. Rev. Lett. **71**, 1994 (1993).
[10] X. Feng *et al.*, Opt. Express **18**, 1316 (2010).
[11] Z. Chang, Appl. Opt. **45**, 8350 (2006).
[12] H. Mashiko *et al.*, Appl. Phys. Lett. **90**, 161114 (2007).
[13] J. Itatani *et al.*, Phys. Rev. Lett. **88**, 173903 (2002).
[14] Y. Mairesse and F. Quere, Phys. Rev. A **71**, 011401(R) (2005).
[15] H. Wang *et al.*, J. Phys. B **42**, 134007 (2009).
[16] V. Yanovsky *et al.*, Opt. Express **16**, 2109 (2008).
[17] X. Zhang *et al.*, Nature Phys. **3**, 270 (2007).
[18] J. Seres *et al.*, Nature Phys. **3**, 878 (2007).